*S. Taheri**

Low-Cycle Fatigue Damage Cumulation Rule for Nonproportional Loading

REFERENCE Taheri, S., **Low-cycle fatigue damage cumulation rule for nonproportional loading,** *Multiaxial and Fatigue Design*, ESIS 21 (Edited by A. Pineau, G. Cailletaud, and T. C. Lindley) 1996, Mechanical Engineering Publications, London, pp. 283–299.

ABSTRACT In order to determine a damage cumulation rule for the prediction of crack initiation under nonproportional loading, we define a nonproportional steady-state cyclically equivalent to uniaxial steady-state, taking both cyclic stress–strain curve and load history into account. Using the same type of analysis, the model is extended to cases involving overloading. A fundamental difference is demonstrated between imposed stress and imposed strain tests. Three methods are proposed for computing damage cumulation: a general method and two conservative simplified methods, derived from the general method and indicating upper bounds for cumulated damage or lower bounds for the number of fatigue cycles to crack initiation. The validity of methods are demonstrated in cases without macroscopic cracking, notably in crack initiation cases. Since little experimental data is available on crack initiation, the method is applied as it is to a fatigue case. This paper reports the testing of the most conservative simplified method, since for the other cases, exhaustive experimental results are not yet available. In the uniaxial case, the proposed method is compared with a nonlinear method, the Miner damage cumulation rule and experimental data. In the multiaxial case, we consider circular tensile–shear loading and compare the experimental number of fatigue (rupture) cycles with a lower bound suggested by the method. In this paper the cyclic mean stress has been disregarded.

1 Introduction

Miner's rule is the most frequently used to access cyclic loading damage cumulation. For a constant amplitude loading sequence, the cumulated damage is given by : $D = \Sigma_i n_i/N_f(\Delta a_i)$, where $N_f(\Delta a_i)$ is the number of cycles to failure (initiation or rupture) for $\Delta a_i = \Delta\varepsilon_i$ (resp. $\Delta a_i = \Delta\sigma_i$), obtained from Manson–Coffin (resp. Wöhler) curve, and n_i is the number of cycles at this amplitude. Failure occurs for $D = 1$. In the multiaxial case, Δa_i is again an amplitude in terms of von Mises or Tresca equivalent. The equivalent stresses and strains are defined in the case of a tensile-shear test by

$$\sigma_e = (\sigma^2 + 3\tau^2)^{1/2} \qquad \varepsilon_e = (\varepsilon^2 + \gamma^2/3)^{1/2} \quad \text{Mises}$$

$$\sigma_e = (\sigma^2 + 4\tau^2)^{1/2} \qquad \varepsilon_e = (\varepsilon^2 + 4\gamma^2/2)^{1/2} \quad \text{Tresca}$$

where σ is the axial stress, ε the axial strain, τ the shear stress and γ twice the shear strain.

*Département de Mécanique et Modélés Numériques, Etudes et Recherches, Electricité de France, 1 Avenue du Général de Gaulle, 92141 Clamart Cedex, France.

The Miner's rule does not take into account the sequence effect (**1–3**). Mainly nonlinear models have consequently been proposed to take this effect into account. However, they seem too complicated and too specific, without really optimizing calculation reliability. In fact Miner's rule may give a better answer than some nonlinear methods (**4**). Damage cumulation can be calculated separately for crack initiation and propagation cases (**2**). Bilinear cumulation rules are then proposed to deal with the sequential effect (**5**). A certain number of problems nevertheless subsist as extension of these models to a nonproportional multiaxial case. It is now relatively well established that the linear cumulation law is suitable for some propagation cases (**2, 6**). The nonlinear part consequently mainly concerns crack initiation, the definition of which is often ambiguous (**7, 8**). However, if the load amplitude is not too low (at least above the true elastic limit, which will be the case in what follows) the end of initiation could be considered to correspond to the sudden coalescence of micro defects in the cell structure walls or the persistent slip bands. In the present paper, we have mainly focused on the crack initiation stage and we shall use N_f to denote the number of initiation cycles in the stress or strain controlled tests, except for the comparison between simulation and experiment where it denotes the number of cycles to rupture.

Our goal has been to propose a damage cumulation method for nonproportional cases (**9**), but our approach to the sequence effect and analysis of the periodic overloading differs from that found in the relevant literature (**2, 3**). We also demonstrate the importance of the type of loading (imposed stress or strain) in such cases. We shall now assume that the Miner's rule holds for an ideal metal on an ideal loading condition, defined by the following two properties

- uniaxial cyclic stress strain curve is stable (independent of prehardening);
- number of cycles to stabilization is negligible compared to the number of cycles to crack initiation.

We shall discuss the consequences of discrepancies with respect to this ideal case, but we first present some experimental results which will be described by the model.

A sequence comprising a high amplitude followed by a low amplitude, H–L is more demaging than the reverse sequence, L–H (**1–3**). These tests are nevertheless usually carried out under strain-controlled conditions. The model proposed confirms this property, but under stress-controlled conditions, it gives the reverse result. Tensile overloading delays crack initiation in a stress-controlled test (**10**). Our model concurs with this property. However, in the case of a strain-controlled test, propagation will be accelerated. Periodic overloading delays crack initiation only in the event of a relatively low overload frequency (**10**). Nonproportional loading is more damaging than equivalent uniaxial loading (in the von Mises or Tresca sense of the term) (**11**), but these are strain-controlled tests. Our model justifies these results, but provides a reverse result in the case of stress-controlled loading (**12**). We shall now suggest a

cumulation method of uniaxial cases and then proceed to its microscopic analysis, which will be extended to include nonproportional and overload cases. We shall then use this microscopic analysis to extend the damage cumulation model to the nonproportional and overload cases.

2 Cyclic Stress–Strain Curves

This chapter deals with cyclic stress–strain curve dependence on cyclic prehardening in both uniaxial and nonproportional contexts. As will be seen from the relevant literature, it has been concluded that a consequence of the formation of stable microscopic structures, such as cell structures, is that the cyclic curve remains stable for values below the loads which created the structures. The formation of such stable structures is directly related to the cross-slipping propensity and for F.C.C. metals; it is consequently related to the stacking fault energy. It is then possible to rank the cyclic stress–strain curves for certain metals in increasing order of dependence on load history: Cu–30%Zn $\gamma = 6$ mJ/m^2; 316 stainless steel $\gamma = 30$ mJ/^{m2}; Cu $\gamma = 90$ mJ/m^2; Al $\gamma = 200$ mJ/m^2 (6). A mild steel (13) included in our analysis features a cross-slipping propensity because of its B.C.C. crystallographic structure.

2.1 *Effect of cyclic prehardening on the cyclic curve*

Figure 1 constitutes the core of this paper. It shows the cyclic stress–strain curves for 316L steel at room temperature, obtained in uniaxial tensile–compressive strain-controlled test. Curve A is a cyclic curve obtained by increasing amplitude level on the same sample. Curve B is the cyclic curve obtained by decreasing amplitude level from point H. Curve C is the cyclic curve obtained by increasing amplitude level from point N. B and C are practically identical. This test demonstrates that the memory of low amplitudes

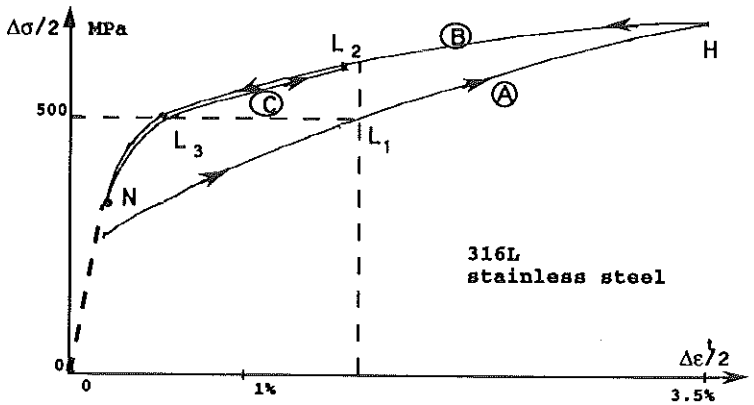

Fig 1 Cyclic strain–stress curve with and without prehardening.

is erased by high amplitudes and the memory of high amplitudes is perfectly preserved at low amplitudes. Curve A can, in practice, be obtained using several samples (**14**, **15**). Curves similar to A–B curves are obtained for maximum amplitudes (point H) equal to $\Delta\varepsilon/2 = 1\%$, 2%, 2.5%, 3% (**15**), but for low amplitudes, $\Delta\varepsilon_p/2 < 0.4\%$ (**16**) or $\Delta\varepsilon/2 < 0.4\%$ (**17**) curves A and B are superimposed. In the nonproportional case, the hardening obtained can be 70% greater than in the equivalent uniaxial case (tests for $\Delta\varepsilon/2 < 4\%$) (**11**, **18**), with a 10% discrepancy on the stress amplitude, depending on whether the von Mises or the Tresca definition is used (**19**). As in the uniaxial case, the maximum loading amplitude effect is very pronounced. On the other hand, unlike the uniaxial case, the cyclic curve is not stable for $\Delta\varepsilon_p/2 < 0.4\%$ (**16**), but at this amplitude range, there is always overhardening in the nonproportional case.

Similar results are obtained for copper, with $\Delta\varepsilon/2 < 1.6\%$ (the maximum amplitude remaining at 1.6%) (**20**). In the nonproportional case, as compared with the uniaxial case, experimental results reveal about 40% overhardening. A hardening discrepancy of around 15% on the stress amplitude is observed, depending on whether the von Mises or the Tresca definition is used. For low plastic strain amplitudes, $0.1\% < \Delta\varepsilon_p/2 < 0.2\%$, the cyclic stress–strain curve is shown to be independent of prehardening in the uniaxial case (**21**). However, in the nonproportional case, hardening can be 50% higher than in the uniaxial case, even for $\Delta\varepsilon_p/2 < 0.2\%$.

Similar results are obtained for a carbon steel (**6**) and for 18G2A and 21CrMoV57 steel, for strain amplitudes of between $0.5\% < \Delta\varepsilon_p/2 < 3\%$ (**22**). For mild steel (**13**), hardening is found to be 30% higher in the nonproportional case than in the uniaxial case (experiments for $\Delta\varepsilon/2 < 1\%$). As compared with a 316 steel, prehardening dependence is much lower. For pure aluminium, the cyclic curve is practically independent of the load history. For this material the uniaxial and nonproportional cyclic curves have been shown to be superimposed (experiments for $\Delta\varepsilon_p/2 < 0.1\%$) (**23**).

In the following analysis we do not differentiate cyclic curves given in total strain and in plastic strain, because it does not change our qualitative analysis.

2.2 *Microstructural analysis under cyclic loading*

Pure copper is the metal which has been the most extensively investigated (**24–26**). In a steady state, the microstructure is dependent on loading amplitude. Low amplitudes will create strain-hardened areas mainly constituted of primary dislocations. Increasing amplitudes produce successively vein structure, persistent slip bands and culminates in cell structure for higher amplitudes when a secondary system is activated.

A comparative analysis of microstructures and cyclic stress–strain curves was performed on stainless steel, copper and aluminium, with proportional and nonproportional loading scenarios (**23**). The overloading effect observed in the case of stainless steel and copper is related to the transformation of a planar

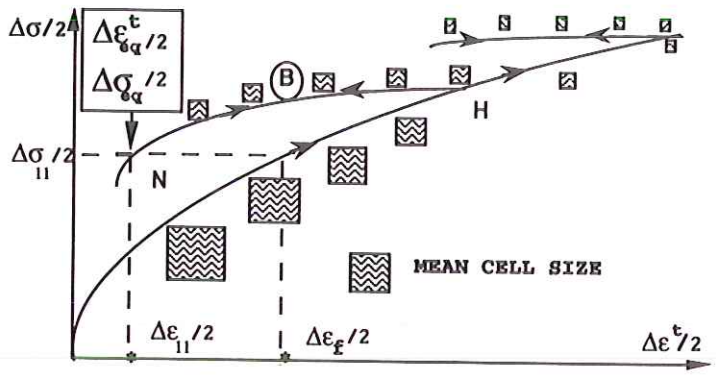

Fig 2 Nonproportional steady-state cyclically equivalent to a uniaxial steady-state.

structure into one containing persistent slip band and, in the nonproportional case, to cell structures resulting from the preferential activation of a second slip system. So the lack of overhardening effect in the case of aluminium (**23**) is related to the fact that cell structures are consistently present, even for low amplitudes. Moreover, it is shown (**19**) that mild steel microstructures under uniaxial and nonproportional cyclic loading are similar, which is not the case for 316 stainless steel. However the situation of curve B with respect to curve C can be explained by the fact that the mean cell size varies according to the loading amplitude (**19, 25, 27**) and that cell structure is relatively stable for amplitudes below that at which it was formed, even if this stability is not perfect (**27**), Figs 1, 2. In the case of aluminium the cyclic curve stability can then be more precisely explained by postulating the existence of a minimum cell mean size, obtained for relatively low loading amplitudes. Some authors (**19, 14, 28**) relate overhardening irreversibility (comparison between A and B curves) at high loading amplitudes to twinning. But this provides only a partial explanation. Results reported in (**29**) show that cell structures are obtained for a 316L steel cycled at $\Delta\varepsilon/2 = 1\%$ without twinning (which only occurs if there is also 3.7% prehardening), whereas the relative A and B situation arises for a maximum strain amplitude of $\Delta\varepsilon/2 = 1\%$ (**15**).

We can conclude finally that for a metal with very easy cross-slipping the three following properties are equivalent

(1) uniaxial cyclic curve independent of prehardening;
(2) mean cell size stabilized at minimum size;
(3) nonproportional cyclic curve and uniaxial cyclic curve are superposed.

3 A Nonproportional Steady-State Cyclically Equivalent to a Uniaxial Steady State

For the case of a 316L stainless steel, as shown in Fig. 2, curve B, cell size is stable for all amplitudes below that of point H. So the metal defined by curve

B is in the same situation as pure aluminium. It means that the uniaxial and the nonproportional cyclic curves are superimposed. This brings us to the following definition.

We define a nonproportional steady state as being *cyclically equivalent* to a uniaxial stabilized state when the mean cell size is identical in both cases.

In practice that means, for the 316L steel, a steady state defined by $(\Delta\varepsilon_{eq}, \Delta\sigma_{eq})$, corresponding to point N on Fig. 2, is equivalent to a steady state obtained by $\Delta\varepsilon_{11} = \Delta\varepsilon_{eq}$ (strain controlled) or $\Delta\sigma_{11} = \Delta\sigma_{eq}$ (stress controlled) with prehardening up to stabilization at point H.

It is clear in the context of metals having a stable cyclic curve, the notion of cyclically equivalent and the usual notion of equivalence defined by von Mises or Tresca rules are identical.

4 Cumulation Rule (Metal with a Nonstable Cyclic Curve)

4.1 *Uniaxial case*

We consider two constant-amplitude loading sequences per block: low- followed by high-amplitude, L–H and the reverse sequence, H–L.

Controlled strain tests

For the sequence L–H, stabilization for load L corresponds to point L_1, and for load H, to point H (Fig. 1). So the cumulated damage for the sequence is:

$$D^{\varepsilon}_{(L-H)} = n_L/N_f(\Delta\varepsilon_L) + n_H/N_f(\Delta\varepsilon_H) \tag{1}$$

Linear cumulation in this case seems reasonable since, as explained in the previous chapter, the memory of load L is erased by load H. D^{ε} means that the computation uses a Manson–Coffin curve. If we apply the sequence H–L, the stabilization points will be H and L_2 (transient cycles having been disregarded for the damage cumulation). We then have to take into account the impact of the memory of load H on load L. In the latter case, we define the cumulated damage as

$$D^{\varepsilon}_{(H-L)} = n_L/\tilde{N}_f(\Delta\varepsilon_L) + n_H/N_f(\Delta\varepsilon_H) \tag{2}$$

where $\tilde{N}_f(\Delta\varepsilon_L)$ is the number of cycles to initiation obtained after cyclic prehardening up to stabilization at point H. So the cumulated damage for a H–L sequence is larger than for the L–H sequence, since the stress amplitude is greater at point L_2 than at point L_1, for identical strain amplitudes. We thus obtain the result usually presented in the relevant literature. Fatigue curves with prehardening are rare in the literature. If we want to use a usual fatigue curve to compare damage created by H–L (L_2) and L–H (L_1) sequnces, we are obliged to use a Wöhler curve

$$D^{\sigma}_{(H-L)} > D^{\sigma}_{(H-L)}$$

Note that in the previous analysis we implicitly assumed that Wohler and Manson–Coffin curves correspond to each other through cyclic stress strain curve. However this is not always exact, but it may be related (**30**) to transitory cycles which have been neglected here.

Controlled stress tests

As in the previous case, the L–H sequence gives points L_1 and H and the H–L sequence gives points H and L_3. Contrary to the previous case the cumulated damage for a H–L sequence is smaller than for the L–H sequence, since the strain amplitude is greater at point L_1 than at point L_3, for identical stress amplitudes. This shows that the H–L sequence is less damaging than the L–H sequence. This is consistent with the fact that the prevailing factor in crack initiation is the strain as far as the propagation stage II has not been reached.

4.2 *Nonproportional case*

When the cyclic stress–strain curve is independent of prehardening, for each uniaxial and nonproportinal cycle, the damage produced (prior to propagation) is assumed to be the same.

This seems normal as a first approximation, since everything depends on the steady state. We have no comparison between uniaxial and nonproportional fatigue curves for aluminium to substantiate this assumption. However, if we disregard the loading anisotropy effect (**18**), these two curves are shown to be practically identical (**19**, **13**), for a mild steel compared with a stainless steel. For the latter, overhardening of the nonproportional case with respect to the uniaxial case is much higher. On this basis, we formulate the following assumption for metals with a non-stable cyclic curve.

In the nonproportional case, the damage produced for each steady state cycle $(\Delta\varepsilon_{eq}, \Delta\sigma_{eq})$ is identical to that of the cyclically equivalent uniaxial case defined in the previous chapter.

With this definition the damage after n cycles at steady state $(\Delta\varepsilon_{eq}, \Delta\sigma_{eq})$ (Fig. 2 point N), is $n/\tilde{N}_f^H$ where $\tilde{N}_f^H$ is the number of cycles to initiation for the uniaxial range $\Delta\varepsilon_{11} = \Delta\varepsilon_{eq}$, (resp. $\Delta\sigma_{11} = \Delta\sigma_{eq}$) under strain controlled conditions (resp. stress controlled conditions) with a stabilization at point H. From this it can be concluded:

In a strain-controlled context, the damage is greater at each cycle with nonproportional loading than in the equivalent uniaxial case, whereas, in a stress-controlled context, the reverse result is obtained (see 4.1).

There are no crack initiation results to invalidate or confirm this analysis, but experimental fatigue test results show that, under strain control, nonproportional loading is more damaging than the equivalent uniaxial loading (**19**). On the other hand, comparative results are practically nonexistent under stress control. However, a result is reported in (**12**), where the nonproportional fatigue

curve is above that corresponding to the uniaxial case (but with different frequencies in both directions).

The above analysis can also be used to explain other cyclic phenomena. For instance, in the strain control test mentioned above, if we plot the steady stress amplitude versus the number of cycles to failure (**19**), the associated fatigue curve will be located above the uniaxial curve. We can derive from the above analysis a cumulated damage upper bound using only uniaxial fatigue curves: we can apply $\Delta\sigma_{eq}$ (Fig. 2) directly on the Wöhler curve, or $\Delta\varepsilon_{eq}$ on a Manson–Coffin curve with cyclic prehardening, or $\Delta\varepsilon_{ef}$, on a Manson–Coffin curve without prehardening. (The latter is used in Section 7 for comparison with the experiment.)

5 Simplified Cumulation Rule for Overloading

The effect of 20% prehardening is examined on the cyclic curve for a 316 steel (**14**) and is observed to raise the cyclic stress–strain curve. The effect is more significant for $\Delta\varepsilon/2 = 0.5\%$ cyclic amplitude than for $\Delta\varepsilon/2 = 1.8\%$ cyclic amplitude. The same effect is reported in (**31**). On the other hand, in the case of copper, 20% prehardening has only a negligible effect on the cyclic curve and we have to reach 40% to obtain a tangible effect (**6**). For a planar system, such as α-brass, 20% prehardening has a much stronger effect than for 316 steel (**6**). In the case of copper, the cells are shown to be formed under substantial monotonic loading (**6**), whereas for aluminium, the cells are formed under practically any loads. For an α-iron, it is shown (**32**) that the cells are formed under monotonic loading and that their mean size decreases as the loading increases (for tests between 2.5 and 7%).

The mean cell size under cyclic loading could then be assumed to be defined approximately by the maximum stress (in absolute value) to which the material had been subjected. The greater this stress, the smaller will be the cell structures. Overloading consequently reduces cell size and implies, as explained in Section 3, that the cyclic curve with prehardening will be above that without prehardening. However the mean cell size is never smaller than that obtained under stabilizing on a range equal to twice the overload. The cyclic curve will consequently be below that obtained after stabilization on a range ($\Delta\sigma_H$ or $\Delta\varepsilon_H$, Fig. 3), equal to twice the overload (σ_{max} or $\Delta\varepsilon_{max}$, Fig. 3). On the other hand we may assume that (see 4.1), if the two strains (resp. stresses) amplitudes are identical, the one with the larger stress (resp. strain) amplitude is more damaging. We then conclude the following relations.

$$D^{\varepsilon}(L_3) < D^{\varepsilon}(P'') < D^{\varepsilon}(L_1) = D^{\sigma}(L_1) < D^{\sigma}(P') < D^{\sigma}(L_2) = D^{\varepsilon}(L_2) < D^{\varepsilon}(L_4)$$

D^{ε}, and D^{σ} show that we have to use respectively a Manson–Coffin curve or a Wöhler curve. Under a stress control test, a **single overload** delays initiation because $D^{\varepsilon}(P'') < D^{\varepsilon}(L_1)$. On the contrary, under strain control test (which is

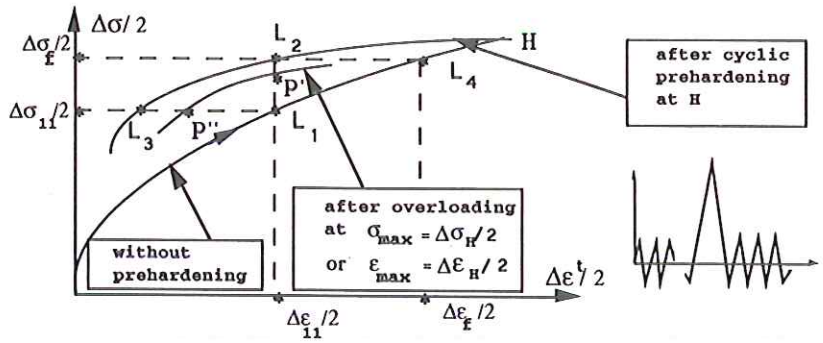

Fig 3 Effect of overloading on cyclic curve.

that applicable to *thermal loads*), an overload accelerates initiation because $D^{\sigma}(L_1) < D^{\sigma}(P')$.

We can propose an upper bound of damage applicable in the event of overloading. Under cyclic stress control condition point P″ is replaced by L_1 (Fig. 3) and a Manson–Coffin curve is used with $\Delta\varepsilon_{11}$. Under cyclic strain control condition, P′ is replaced by L_2 and a Wöhler curve is used with $\Delta\sigma f$, or P′ is replaced by L_4 in which case a Manson–Coffin curve is used with $\Delta\varepsilon f$. In the case of a metal for which the cyclic curve is independent of prehardening, the number of cycles to crack initiation will be unaffected by the overload.

In the case of a **periodic overload**, we can conclude (**33**) that, the number of cycles to crack initiation will increase only if the relative frequency of occurrence of overloading is low. This result is consistent with those concerning the effect of periodic overloading on crack propagation (**10**).

6 Non-Negligible Transient Cycles

The analysis in Section 4 provides no explanation as to why, in L–H sequence under strain control conditions, we have $\Sigma_i n_i/N_f(\Delta a_i) > 1$ (**1**, **2**, **4**). This may be probably explained (**33**) by a greater importance of transitory cycles in an L–H sequence than in a H–L one.

Taking into account the transitory cycles, we have proposed also a damage cumulation rule for progressive deformation (**30**) in cases where the direct incidence of mean strain on damage cumulation is disregarded (it has been taken into account only through the mean stress).

A random load is constituted essentially of transitory cycles. The method described in Fig. 3 may be applied. As before, the Miner rule may give a good response compared with nonlinear models, if the cyclic curve is stable. This seems to be the case in (**4**) where the metal seems to have a stable cyclic curve (**34**).

7 Comparison with Experiment and Other Models

7.1 *Uniaxial case with alternating tensile–compressive straining*

The aforementioned method is applied as it is to a fatigue case, due to the lack of corresponding experimental data on crack initiation. We propose three damage cumulation methods: a general method and two simplified conservative methods. For the simplified methods, under strain control, we replace point L_1 by L_2 (Fig. 3) and then use a Wöhler curve, or we replace L_1 by L_4 and then use a Manson–Coffin curve. In the latter case, we obviously obtain a more conservative response. This second method is used here for purposes of comparison, since less complete sets of experimental results are available for the other cases. Here we compare, through a two-amplitude block loading, our method with experiments and also with Miner's rule using a Miner diagram. In this diagram, our simplified model is represented by a line AB (the tests begin with the larger amplitude), Fig. 5d. The general model is represented by a multilinear curve of BMNP type, Fig. 5c.

Experimental results, and nonlinear method

The fatigue experiments used (35) concern an AISI 316 steel, Z3 CND 17–12, at room temperature, under uniaxial alternating tensile–compressive stress. Two types of loading are used, K and L, Fig. 4. In both cases, testing begins with the high amplitude cycles. These results have been compared (35) with the nonlinear method of Marco and Starkey (36). The paired amplitudes concerned ($\Delta\varepsilon_H/2$, $\Delta\varepsilon_L/2$) are as follows: (1%, 0.3%) for K or L-type loading, (1%, 0.2%)

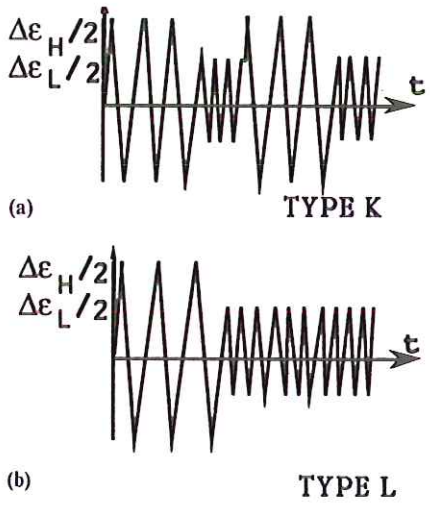

Fig 4 Types of loading sequences.

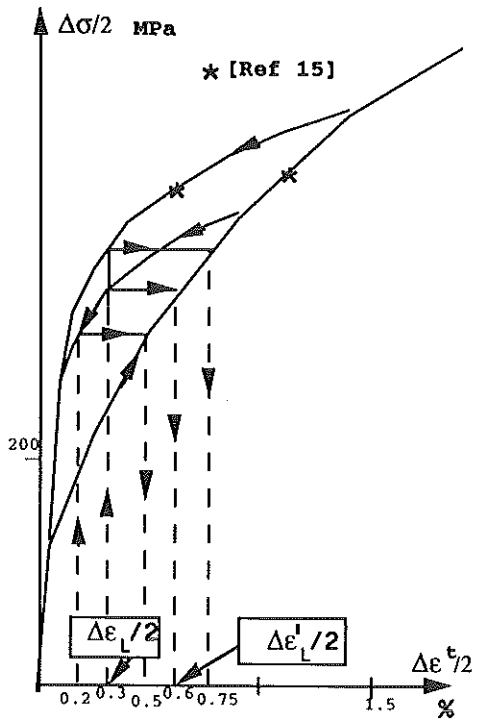

Fig 5 (a) Cyclic curves with and without prehardening for a 316 stainless steel.

for L-type loading, and (1.5%, 0.3%) for K-type loading. To compare our method to these experiments, we need cyclic stress–strain curves with cyclic prehardening. Such curves are available for the above-mentioned 316 steel, Fig. 1, and for another 316 steel in (**14**). In Fig. 1, the cyclic stress strain curve with cyclic prehardening corresponds to the maximum amplitude given by $\Delta\varepsilon/2 = 3.5\%$, which does not relate to fatigue tests (**35**). So we use the cyclic curves in document (**14**), however this surely gives rise to some error.

The proposed method

The most conservative simplified method is summarized as follows, Fig. 5a.

(1) at failure, we have n_H high amplitude cycles and the associated damage fraction is $n_H/N_f(\Delta\varepsilon_H)$;
(2) we calculate the fictitious amplitude $(\Delta\varepsilon'_L/2)$ associated with the small amplitude $(\Delta\varepsilon_L/2)$;
(3) we calculate $N_f(\Delta\varepsilon'_L/2)$ the number of cycles to failure associated with the fictitious amplitude $(\Delta\varepsilon'_L/2)$ by a Manson–Coffin curve.

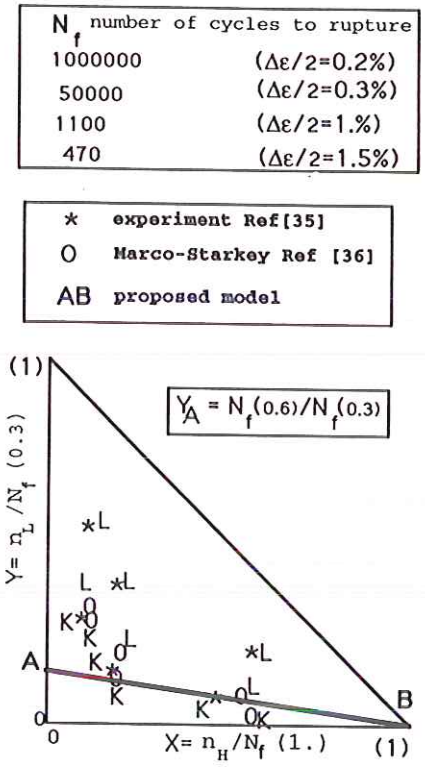

Fig 5 (b) Loadings type K and L.

On the Miner diagram, we then define the linear function:

$$Y = [N_f(\Delta\varepsilon'_L/2)/N_f(\Delta\varepsilon_L/2)](1 - X) \tag{4}$$

noted AB (Figs. 5b,c,d). This third stage is justified by the following equation.

$$n_H/N_f(\Delta\varepsilon_H/2) + n'2/N_f(\Delta\varepsilon'_L/2) = 1 \tag{5}$$

$$Y = n'2/N_f(\Delta\varepsilon_L/2)] \tag{6}$$

Equation (5) traduces the fact that the cyclic curve B, Fig. 1, is stable and that as we supposed, Miner's rule is valid when the cyclic curve is stable. It has to be noted that our method gives a conservative result, and that loadings L and K are not discriminated.

Through (**35**), we find that the number of fatigue cycles for the amplitudes of strain $\Delta\varepsilon/2 = 1.5\%$, 1%, 0.3%, 0.2%, are respectively 470, 1100, 50 000, 1000 000. The first comparison concerns the couple ($\Delta\varepsilon_H/2 = 1\%$, $\Delta\varepsilon_L/2 = 0.3\%$). The lower bound of number fatigue cycles in our model is

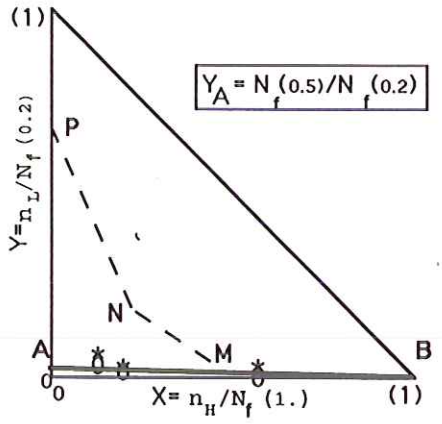

Fig 5 (c) Loading type L.

presented by the line AB (Fig. 5b), where we obtain $\Delta\varepsilon'_L = 0.6$, Fig. 5a. The other results are shown on Figs 5c and d.

7.2 *Nonproportional case*

For this case, we shall use the results of (**11, 19**), which report nonproportional loading tests on a 316L steel Z3CND 17–12, involving circular tensile–shear loads applied under strain-controlled conditions. This type of loading is considered to give the highest overhardening and consequently creates the largest

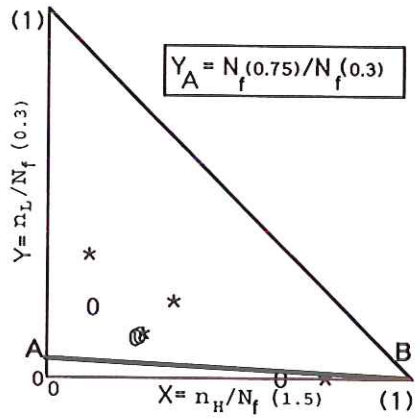

Fig 5 (d) Loading type K.

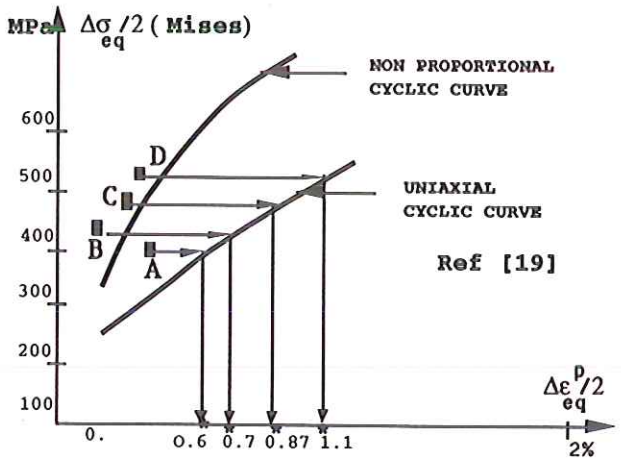

Fig 6 A uniaxial amplitude equivalent to the nonproportional one.

damage under strain-controlled conditions (the equivalent mean stress in this case being zero). Figure 6 shows uniaxial and nonproportional cyclic stress–strain curves (**19**), on which we have kept only the steady-state points A, B, C, D, associated with the different types of circular loading, for which elastic strain is easily computed. The number of cycles to failure are respectively, 4000, 3818, 2624, 1612, Fig. 7.

Our simplified method for determination of an upper bound for cumulated damage or a lower bound for the number of cycles to failure is summarized below. Taking into account the definition of Section 3, we replace L_2 by L_4 (Fig. 3). This means that we find the upper bounds of strain amplitudes (horizontal lines followed by vertical ones, Fig. 6). The plastic strain amplitudes thus obtained, associated with points A, B, C, D, are respectively 0.6%, 0.7%, 0.87%, 1.1%. We then have to switch to total control strain conditions, since the fatigue curves correspond to this context. The Young's modulus is 183 000 MPa (**19**). For the circular loading cases corresponding to the A, B, C, D tests, we obtain successive elastic strain amplitudes of 0.21%, 0.23%, 0.27%, 0.3%. The total strain amplitudes are consequently, 0.8%, 0.93%, 1.15%, 1.4%. For the first two amplitudes, the number of cycles to failure are found on Fig. 7, equal to 2000 and 1500, respectively. For the other two, we had to use the fatigue curve given in (**34**) and we obtained 900 and 500. The experimental values are respectively, 4000, 3818, 2624, 1612.

We found a ratio of between 2 and 3 for the first two amplitudes and between 3 and 4 for the other two. This result may nevertheless be considered as a creditable achievement, since the safety factor used by ASME on the number of cycles is in the region of 20. The nonproportional result obtained was more conservative than the uniaxial result, whereas the opposite was expected. This

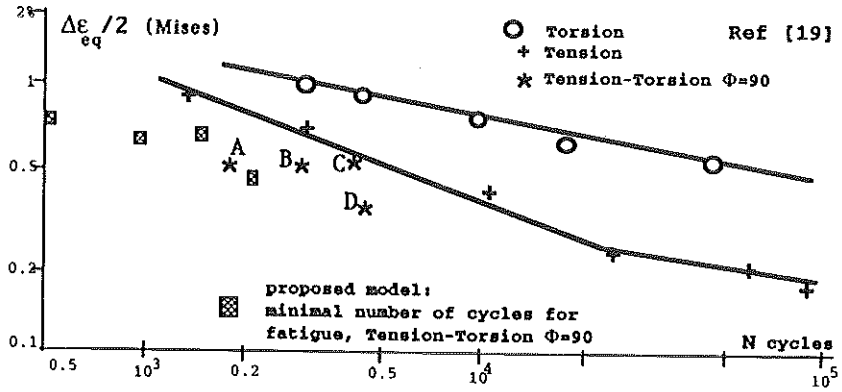

Fig 7 Minimal number of cycles to fatigue for some circular loadings.

may be due to the fact that, in the uniaxial tension–compression case, propagation is easier and that extending this method, which was developed for crack initiation, to entire lifetime assessment, intensifies its conservative tendency in nonproportional cases. *But at the same time, extending this initiation method of lifetime assessment becomes valid in the nonproportional case.*

8 Conclusion

Miner's cumulation rule is assumed to be valid in the event of a stable cyclic stress–strain curve where transient cycles are negligible. It is shown that many experimental effects reported in the relevant literature can be described by their discrepancy with respect to these assumptions. A simplified method of obtaining an upper bound for cumulated damage or a lower bound for the number of cycles for crack initiation, in the event of nonproportional loading and overloading, is proposed. Due to the lack of corresponding data on initiation this method has been applied as it is to fatigue. Comparison with experimental data and a nonlinear method, in uniaxial and nonproportional loading produces satisfactory results. We have also shown an important difference between strain- and stress-controlled tests.

References

(1) MILLER, K. J., ZACHARIAH, K. P. (1977) Cumulative damage laws for fatigue crack initiation and stage I propagation. *J. of Strain Analysis*, **12**, (4), pp. 262–270.
(2) MILLER, K. J. and IBRAHIM, F. E. (1981) Damage accumulation during initiation and short crack growth regimes, *Fatigue of Eng. Mat. and Struc.*, **4**, (3), pp. 263–277.
(3) SUHR, R. W. (1992) Interaction of high-strain and high-cycle fatigue in turbine materials, *Fatigue of Eng. Mat. and Struc.*, **15**, (4), pp. 399–415.
(4) VASEK, A. and POLAK, J. (1992) Fatigue life of two steels under variable amplitude loading, *Proc. VTT Symposium 130, Fatigue Design*, Finland, **1**, pp. 89–98.

(5) MANSON, S. S. and LALFORD, G. R. (1986) Reexamination of cumulative fatigue damage analysis an engineering perspective, *Eng. Frac. Mechanics*, **25**, (5/6), pp. 539–571.
(6) KLESNIL, M. and LUKAS, P. (1980) *Fatigue of Metallic Materials*, Elsevier.
(7) MAGNIN, T. (1991) Développements récents en fatigue oligocyclique sous l'angle de la métallurgie physique, *Mémoires et études scientifiques, revue de métallurgie*, pp. 33–48.
(8) MILLER, K. J. (1991) Metal fatigue past, current and future, *Proc. Institution of Mechanical Engineers*, No. 3.
(9) TAHERI, S. (1991) A damage cumulation law under nonproportional cyclic loading with overloads for the prediction of crack initiation, *Proc. Plasticity* 91, *3rd Int. Symposium on Plasticity and its Current Applications*, (Boehler, J. P./Khan, A. S., Eds)., Grenoble, France, Elsevier Ed., pp. 459–462.
(10) OHRLOF, N., GYSLER, A. and LUTJERING, G. (1987) Fatigue crack propagation behaviour under variable amplitude loading, *Proc. 3rd Int. Conf. on Fatigue Crack Growth Under Variable Amplitude Loading*, Paris, (Ed. Petit, J., Davidson, D., Suresh, S., Rabbe, P.,) **1**, pp. 18–23.
(11) CAILLETAUD, C., DOQUET, V. and PINEAU, A. (1989) Prediction of macroscopic multiaxial behaviour from microstructural observations, *Proc. 3rd Int. Conf. on Biaxial/Multiaxial Fatigue*, (Ed. Kussmaul, K., Stuttgart, F. R. G.,) **1**, pp. 25.1–25.19.
(12) MacDIARMID, D. L. (1989) The effect of mean stress on biaxial fatigue where the stresses are out-of-phase and at different frequencies, *Proc. Biaxial/Multiaxial Fatigue*, (Ed. Brown, M. W./Miller, K. J.,) EGF Publication 3, pp. 605–619, Figure 4, Curves 5 & 6.
(13) DOQUET, V. and PINEAU, A. (1989) Multiaxial low cycle fatigue behaviour of a mild steel, *Proc. 3rd Int. Conf. on Biaxial/Multiaxial Fatigue*, (Ed., Kussmaul, K., Stuttgart, F. R. G.,) **1**, pp. 23.1–23.19.
(14) LIEURADE, H. P., RIBES, A. and BOLLINGER, E. (1986) Influence d'un préécrouissage sur le comportement d'un acier Z2CND 17–13 (AISI 316L) en fatigue oligocyclique, *Mémoires et Etudes Scientifiques Revue de Metallurgie*, pp. 547–551.
(15) CHABOCHE, J. K., DANG VAN, K., and CORDIER, G. (1979) Modelisation of the strain memory effect on the cyclic hardening of 316 stainless steel, S.M.I.R.T., L11/3, Berlin.
(16) TANAKA, E., MURAKAMI, S. and OOKA, M. (1985) Effects of strain amplitudes on nonproportional cyclic plasticity, *Acta Mech.*, **57**, pp. 167–182.
(17) MURAKAMI, S., KAWAI, M., AOKI, K. and OHMI, Y. (1989) Effects of amplitude-history and temperature history on multiaxial cyclic behaviour of 316 stainless steel, *Trans. of ASME. J. of Eng. Mat. & Technology*, **111**, pp. 32–39.
(18) BENALLAL, A., CAILLETAUD, C., CHABOCHE, J. L., MARQUIS, D., NOUAILAS, D. and ROUSET, M. (1989) Description and modelling of nonproportional effects in cyclic plasticity, *Biaxial and Multiaxial Fatigue*, (Ed. Brown M. W. and Miller K. J.,) EGF Publication 3, pp. 107–129.
(19) DOQUET, V. (1989) Comportement et endommagement de deux aciers à structure cubique centrée et cubique à faces centrées, en fatigue oligocyclique, sous chargement multiaxial non proportionnel. Thèse de Doctorat, Ecole des Mines de Paris.
(20) LAMBA, H. S. and SIDEBOTTOM, O. M. (1978) Cyclic plasticity for nonproportional paths Part I, cyclic hardening, erasure of memory, and subsequent strain hardening experiments, *Trans. of ASME, J. of Eng. Mat. & Technology*, **100**, pp. 96–103.
(21) FIGEUR, J. C. and LAIRD, C. (1981) The cyclic stress/strain response of copper at low strain variable testing, Part II. *Acta Met.*, **29**, pp. 1679–1684.
(22) TRAMPCZYNSKI, W. (1988) The experimental verification of the evolution of kinematic and isotropic hardening in cyclic plasticity, *J. Mech. Phys. Solids*, **36**, (4), pp. 417–441.
(23) DOONG, S. H. and SOCIE, D. F. (1989) Deformation mechanisms of metals under complex nonproportional cyclic loadings, *Proc. 3rd Int. Conf. on Biaxial/Multiaxial Fatigue*, (Ed., Kussmaul K.), Stuttgart, FRG) **1**, pp. 12.1–12.20.
(24) GROSSKREUTZ, J. C. (1971) The mechanisms of metal fatigue (I), *Phy. Stat. Sol.*, (b) **47**, (11).
(25) GROSSKREUTZ, J. C. and MUGHRABI, M. (1975) Description of workhardened structure at low temperature in cyclic deformation, *Constitutive Equations in Plasticity*, (Ed. Argon A. S.), M.I.T Press.
(26) MUGHRABI, H. (1985) Dislocations in fatigue, *Proc. Conf. on Dislocations and Properties of Real Materials*, Institute of Metals, London, publication No 323, pp. 244–262.
(27) ERMI, A. M. and MOTEFF, J. (1983) Microstructural development of AISI 304 stainless steel tested in time-dependent fatigue modes. *J. of Eng. Mat. & Technology*, **105**, pp. 21–30.

(28) DOQUET, V. (1992) Deformation twinning and cyclic behaviour of a CoNi alloy under multiaxial loading, *Multiaxial Plasticity*, MECAMAT '92, Paris.
(29) DONADILLE, B. C., ESSADIGI, L., PERNOT, M. and PENELLE, R. (1978) Etude de l'évolution de la microstructure et de la texture cristallographique d'acier inoxydable 316L au cours de chargements unidimensionnels monotones et/ou cycliques, *Proc. Matériaux et Structures sous Chargement Cyclique*, Palaiseau, France, pp. 91–94.
(30) TAHERI, S. (1992) A modified Miner rule to predict crack initiation, *Proc. VTT Symposium P130, Fatigue design*, Finland, **1**, pp. 111–125.
(31) JACQUELIN, B., HOURLIER, F. and PINEAU, A. (1983) Crack initiation under low-cycle multiaxial fatigue in type 316L stainless steel, *J. Pres. Vessel Technology*, **105**, pp. 138–143.
(32) BENARD, J., MICHEL, A., PHILIBERT, J. and TALBOT, J. (1984) Métallurgie générale (Ed. Masson,) pp. 224.
(33) TAHERI, S. (1993) Une règle de cumul de dommage, Miner modifiée, pour la fatigue oligocyclique, *J. Printemps, Société Française de Métallurgie et de Matériaux*, Paris, pp. 281–293.
(34) VASEK, A. and POLAK, J. (1991) Low cycle fatigue damage accumulation in Aramco-iron, *Fatigue and Frac. of Mat. & Struct.*, **14**, (2/3), pp. 193–204.
(35) BAUDRY, G., AMZALLAG, C. and BERNARD, J. L. (1984) Etude du cumul de dommage en fatigue sur un acier austénitique, *J. Printemps, Société Française de Métallurgie et de Materiaux*, Paris, commission de fatigue des métaux modulus.
(36) MARCO, S. M. and STARLEY, W. L. (1954) A concept of fatigue damage, *Trans. of AMME*, **76**, p. 672.